Development and performance assessment of post-combustion emission control device, embedded with breadfruit pulp biochar

Obiora Nnaemeka Ezenwa[1]

Mmesoma Echezonachukwu Echeta[2]

John Chikaelo Okeke[3+]

Arinze Everest Chinweze[4]

Chibuzo Ndubuisi Okoye[5]

Augustine Uzodinma Madumere[6]

[1,2,3,4,5,6]*Department of Mechanical Engineering, Nnamdi Azikiwe University, Awka, Nigeria.*
[1]*Email: on.ezenwa@unizik.edu.ng*
[2]*Email: echetammesoma@gmail.com*
[3]*Email: jc.okeke@unizik.edu.ng*
[4]*Email: ae.chinweze@unizik.edu.ng*
[5]*Email: cn.okoye@unizik.edu.ng*
[6]*Email: au.madumere@unizik.edu.ng*

(+ Corresponding author)

ABSTRACT

This study presents the design, fabrication, and experimental evaluation of a small-scale carbon capture device aimed at mitigating exhaust emissions from petrol generators. Motivated by Nigeria's heavy dependence on fossil fuels and the associated greenhouse gas (GHG) emissions, the research explores the use of breadfruit pulp–derived biochar as a low-cost, sustainable adsorbent for post-combustion carbon dioxide (CO_2) capture. The carbon capture system was developed using stainless-steel chambers arranged in series, each packed with graded biochar particles to enhance gas–adsorbent contact. Theoretical design analyses and SolidWorks static simulations were performed to verify the structural adequacy under combined thermal (600 °C) and pressure (7 kPa) loads. Experimental results using an air quality detector showed significant reductions in CO and CO_2 emissions, demonstrating the biochar's adsorption efficiency. Simulation outcomes indicated minimal deformation and confirmed the mechanical stability of the capture unit, although localized stress concentrations suggested a need for minor design improvements. Overall, the study validates the feasibility of using agricultural waste–derived carbon materials for emission control, offering a sustainable solution for small-scale power sources in developing regions.

Contribution/Originality: This study contributes to the existing literature by demonstrating how breadfruit pulp biochar can capture generator exhaust emissions. It employs a practical design–simulation–testing approach and develops simple design formulas. As one of the few studies in this area, it documents a low-cost, sustainable method for reducing emissions.

1. INTRODUCTION

The growing global demand for energy, driven by rapid population and industrial expansion, has intensified dependence on fossil fuels as the primary energy source (Wang & Azam, 2024). In developing nations such as

Nigeria, unreliable and erratic electricity supply has compelled many households and businesses to rely heavily on fuel-powered generator sets for their daily power needs (Adenikinju, 2003). While these generators provide short-term energy relief, their extensive use significantly increases the emission of greenhouse gases (GHGs), particularly carbon monoxide (CO) and carbon dioxide (CO_2), which are key contributors to global warming and climate change (Ahmed, Rehan, Basit, & Hong, 2022).

GHGs trap heat in the atmosphere, leading to a rise in global temperature, melting of polar ice caps, sea-level rise, and frequent extreme weather events (El Zein & Chehayeb, 2015). These environmental consequences have prompted urgent global attention toward technologies that can reduce carbon emissions and mitigate climate impacts. Among the available strategies, carbon capture and storage (CCS) has emerged as one of the most promising approaches for reducing CO_2 emissions from fossil-fuel-based sources (Herzog, 2018; Hua, Sha, Zhang, & Cao, 2023; Wilcox, 2012). CCS involves capturing CO_2 at its emission source, such as power plants, cement factories, and generator exhausts, before it escapes into the atmosphere, then transporting and storing it in secure geological formations or converting it into useful products.

Among the different carbon capture routes, post-combustion capture has gained the most attention due to its flexibility and suitability for retrofitting existing systems (Gkotsis, Peleka, & Zouboulis, 2023; Tian, Wang, Zhen, & Liu, 2022). In this method, CO_2 is separated from flue gases after combustion using techniques such as absorption, adsorption, membrane separation, or cryogenic processes (Chao, Deng, Dewil, Baeyens, & Fan, 2021; Peu et al., 2023; Sharma & Tyagi, 2024). Adsorption-based capture, in particular, has shown great potential due to its simplicity, low energy requirement, and reusability of adsorbents (Allangawi et al., 2023). The success of this technique, however, depends largely on the development of efficient, low-cost, and sustainable adsorbent materials.

Conventional adsorbents such as zeolites, metal–organic frameworks (MOFs), and amine-functionalized solids have demonstrated good CO_2 capture capacities but face challenges related to high production costs, complex regeneration, and poor performance in humid environments (Raganati, Miccio, & Ammendola, 2021). In contrast, biomass-derived carbon materials offer a renewable and eco-friendly alternative with desirable characteristics such as high surface area, tunable porosity, thermal stability, and surface functional groups that enhance CO_2 adsorption (González, Plaza, Rubiera, & Pevida, 2013). Additionally, biomass valorization supports waste-to-resource strategies that promote a circular carbon economy.

Biomass from agricultural residues is particularly attractive because of its abundance, low cost, and potential for rural energy sustainability (McKendry, 2002). In this context, breadfruit pulp, a locally available and underutilized agricultural residue, presents a promising precursor for developing porous carbon-based adsorbents. When subjected to controlled pyrolysis, breadfruit pulp can yield a high-surface-area carbon material with microporous structures suitable for CO_2 capture applications. Such bio-derived carbon adsorbents not only provide an environmentally sustainable solution for emission control but also contribute to value addition and waste reduction in agro-based economies.

Therefore, this study aims to develop and characterize carbon materials derived from breadfruit pulp for application in post-combustion CO_2 capture systems. By converting an abundant biomass resource into an efficient carbon adsorbent, this research seeks to provide a cost-effective and sustainable pathway for reducing CO_2 emissions from small- and medium-scale power sources such as household generators and industrial exhausts in Nigeria and beyond.

2. MATERIALS AND METHODS

The carbon capture machine was developed through a combination of graphical and mathematical design, simulation analysis, and fabrication using selected engineering materials that satisfied the required design specifications. The machine was then tested experimentally to evaluate its performance in reducing carbon emissions from a generator exhaust.

2.1. Graphical Design

The carbon capture machine comprises three main compartments, each performing similar functions and arranged in series to enhance gas–adsorbent interaction. The inlet pipe was designed to connect directly to the generator exhaust outlet and welded to a 6-inch diameter port to ensure a tight and secure interface.

Each compartment (port) was modeled in two halves, each measuring approximately 2 inches in length. Between every pair of port halves lies a central drum, enclosed at both ends with fine metal gauze to retain the biochar adsorbent in position. Gaskets were inserted on both sides of the drum to ensure a gas-tight seal, while the port halves were clamped together using bolted flanges for mechanical strength and ease of disassembly during maintenance.

The compartments were interconnected using 2.5-inch-diameter galvanized steel throats. To accommodate flow dynamics, the second port halves were designed to be 0.5 inch shorter than the first halves, thereby compensating for the expected velocity and pressure drop following gas–biochar interaction. The resulting design ensured uniform gas flow distribution, reduced back pressure, and optimized contact time for CO_2 adsorption. Figure 1 presents the section view of the carbon capture machine, showing the arrangement of the three biochar-filled compartments and their structural layout.
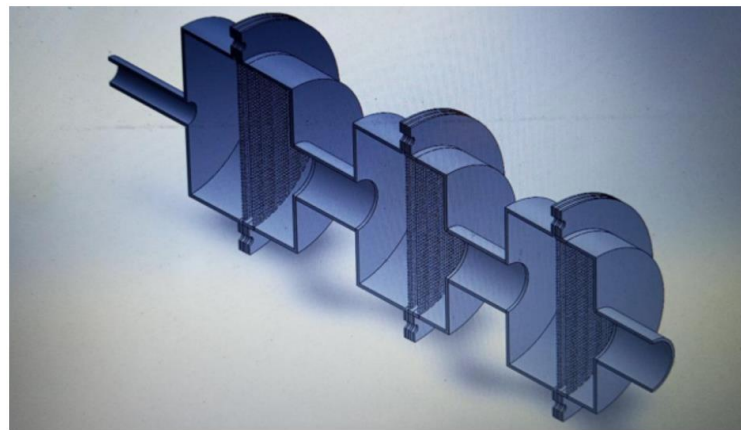

Figure 1. Section view of the carbon capture machine.

2.2. Mathematical Design

Mathematical design analysis was carried out to determine critical parameters required for selecting suitable materials and dimensions for the carbon capture machine. These calculations were essential to ensure that the machine would operate efficiently and safely under anticipated working conditions.

2.2.1. Volume and Dimensions of the Carbon Capture Chamber

Each of the three compartments was designed to hold biochar through which generator exhaust gases would pass for CO_2 capture. The effective volume of each biochar chamber (V_c) and its height (h_c) were determined using the relations.

$$V_c = A \times h_c \tag{1}$$

$$A = \pi \left(\frac{d_c}{2} \right)^2 \tag{2}$$

Where:

d_c = Chamber diameter (6 in).

A = Cross-sectional area of the chamber

These parameters were selected to ensure adequate gas flow pathways while maintaining sufficient adsorbent mass for effective CO₂ capture. The schematic representation of the carbon capture machine and its dimensional layout is shown in Figure 2.
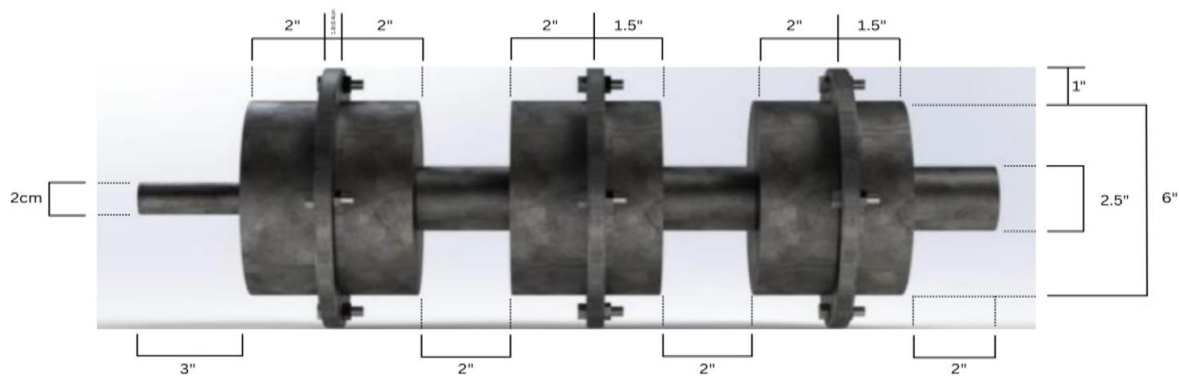

Figure 2. Schematic diagram of the carbon capture machine showing the compartments and dimensional specifications.

Figure 2 illustrates the schematic diagram of the carbon capture machine, highlighting the compartments, flow paths, and dimensional specifications.

2.2.2. Wall Thickness Analysis

The carbon capture machine was fabricated using stainless steel pipe with an internal diameter of 6 in (15.24 cm) and a wall thickness of 0.3 cm. This thickness was chosen to ensure that the structure could safely withstand the dynamic pressure of the exhaust gases without deformation or rupture.

The hoop stress (σ_h) acting on the pipe wall was estimated using the thin-walled pressure vessel relation (Bai & Bai, 2014):

$$\sigma_h = \frac{(P_i - P_o)D}{2t} \qquad (3)$$

Where,

P_i = Internal exhaust gas pressure.

P_o = Atmospheric pressure.

D = Outside diameter of the pipe (15.24 cm + 0.3 cm).

t = Wall thickness (0.3 cm).

The calculated hoop stress was compared with the ultimate tensile strength of stainless steel to confirm that the selected thickness would withstand the applied load safely (Reddy, 2005). This verification ensured the structural integrity of the ports, drums, and connecting throats under operational conditions.
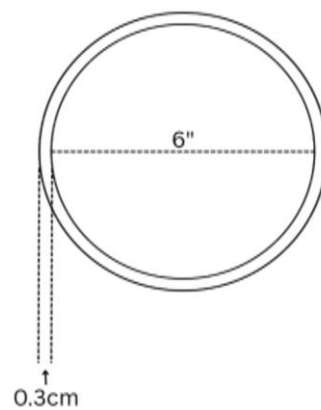

Figure 3. Image of the wall thickness.

Figure 3 shows the image of the stainless-steel wall thickness used for fabricating the carbon capture chambers.

2.3. Fabrication Process

Fabrication followed standard workshop procedures. Stainless steel pipes and galvanized throats were first measured and marked according to the design dimensions. Components were cut, drilled, and welded to form the three main compartments. Gaskets, flanges, and metal gauze were fitted into each chamber to hold the biochar securely and maintain gas-tight seals.

The ports were joined using galvanized steel throats, with dimensional adjustments made to counteract potential pressure and velocity losses. Biochar was then packed into the chambers in decreasing particle sizes from coarse at the inlet to fine at the outlet to enhance gas diffusion and adsorption efficiency while minimizing back pressure.

Surface finishing, including grinding, filing, and sandpapering, was performed to remove weld residues and achieve smooth surfaces. The entire assembly was then spray-painted to prevent corrosion and improve durability. Figure 4 presents half of the device's inlet port, indicating the interface designed to attach the capture unit to the generator exhaust.

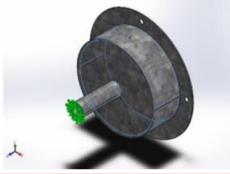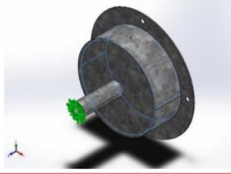**Figure 4.** Half of the device's inlet port.

Load name	Load Image	Load Details
Temperature-1		**Entities:** 3 face(s) **Temperature:** 600 Celsius
Pressure-1		**Entities:** 3 face(s) **Type:** Normal to selected face **Value:** 7,000 **Units:** N/m^2 **Phase Angle:** 0 **Units:** deg

Figure 5. Image of the Simulation input at the maximum operating temperature of 600 °C and a pressure of 7000 N/m².

Figure 5 displays the simulation input conditions, including the applied 600 °C thermal load and 7000 N/m² internal pressure.

2.4. Static Structural Simulation of Inlet Port

To evaluate the mechanical reliability of the inlet port under operating conditions, a static simulation was conducted using SolidWorks Simulation.

124

2.4.1. Geometry Simplification

Only half of the inlet geometry was modeled to reduce computational requirements. Symmetry ensured that the results accurately represented the full structure.

2.4.2. Boundary Conditions

- Fixed Support: One face of the inlet port was constrained to represent the welded connection to the generator exhaust, eliminating translational and rotational degrees of freedom.
- Pressure Load: An internal pressure of 7,000 N/m² (7 kPa) was applied normal to the inner wall, simulating exhaust gas back pressure.
- Thermal Load: A uniform temperature of 600°C was applied to replicate exhaust gas heating effects.

2.4.3. Meshing

A fine mesh was used for improved accuracy in stress and displacement prediction, particularly around curved and fixed surfaces.

Mesh type	Solid Mesh		Total Nodes	28553
Mesher Used:	Blended curvature-based mesh		Total Elements	14054
			Maximum Aspect Ratio	6.0302
Jacobian points for High quality mesh	16 Points		% of elements with Aspect Ratio < 3	97.3
Maximum element size	0.21768 in		Percentage of elements with Aspect Ratio > 10	0
Minimum element size	0.0725591 in		Percentage of distorted elements	0
Mesh Quality	High		Time to complete mesh(hh;mm;ss):	00:00:05
			Computer name:	

Figure 6. Mesh details.

Figure 6 shows the mesh configuration applied during the static structural simulation, highlighting the element density and refinement.

The simulation results were later compared with the analytical hoop stress derived in Section 2.2.2 to validate the mechanical adequacy of the inlet port under combined thermal and pressure loads.

2.5. Testing and Evaluation

Performance evaluation was conducted using a portable Air Quality Detector obtained from Onitsha, capable of measuring concentrations of carbon monoxide (CO), carbon dioxide (CO_2), particulate matter (PM), formaldehyde (HCHO), and total volatile organic compounds (TVOC). Although the primary focus was on CO and CO_2 removal efficiency, the additional parameters were measured to gain broader insight into the exhaust gas composition.

The tests were carried out by connecting the carbon capture machine to a generator exhaust and monitoring the concentration of CO and CO_2 before and after gas passage through the biochar chambers. The adsorption capacity of the biochar was determined under different operational conditions to evaluate the overall filtration performance. The results obtained provided quantitative evidence of the machine's ability to reduce harmful emissions and demonstrated the feasibility of biochar as a sustainable adsorbent material for small-scale carbon capture applications.

3. RESULTS AND DISCUSSIONS

3.1. Preliminary Validation of Measuring Instrument

Before commencing the main experiment, the air quality detector was validated to ensure its accuracy and responsiveness. The detector was first exposed to ambient outdoor air to record the baseline atmospheric concentrations of various parameters. Subsequently, a matchstick was ignited near the detector to simulate a simple

combustion process. The increase observed in the concentrations of carbon monoxide (CO) and carbon dioxide (CO_2) after ignition confirmed that the detector was functioning correctly, as shown in Table 1.

Table 1. Validation of an air quality detector using matchstick combustion.

Parameters	Values
HCHO (mg/m³)	0.395
TVOC (mg/m³)	1.999
PM2.5 (μ/m³)	999
PM10 (μ/m³)	999
CO (PPM)	154
CO_2 (PPM)	3565

Following the validation test, the detector was used to measure the exhaust emissions from a Sumec Firman petrol engine generator set. Readings were taken directly from the exhaust outlet for 10 seconds before inserting the carbon capture device. The results obtained are presented in Table 2.

Table 2. Emission readings from generator exhaust prior to carbon capture integration.

PARAMETERS	Values after t = 10 seconds
HCHO (mg/m³)	1.999
TVOC (mg/m³)	1.999
PM2.5 (μ/m³)	999
PM10 (μ/m³)	999
CO (PPM)	687
CO_2 (PPM)	5000

It is important to note that each parameter reached the maximum measurable limit of the detector, implying that the actual pollutant concentrations exceeded the device's detection capacity. This limitation introduces uncertainty in determining the precise emission levels before the carbon capture intervention. However, the observed saturation trend validates the detector's sensitivity to high-concentration combustion gases, confirming its suitability for relative comparative analysis during subsequent experimental stages.
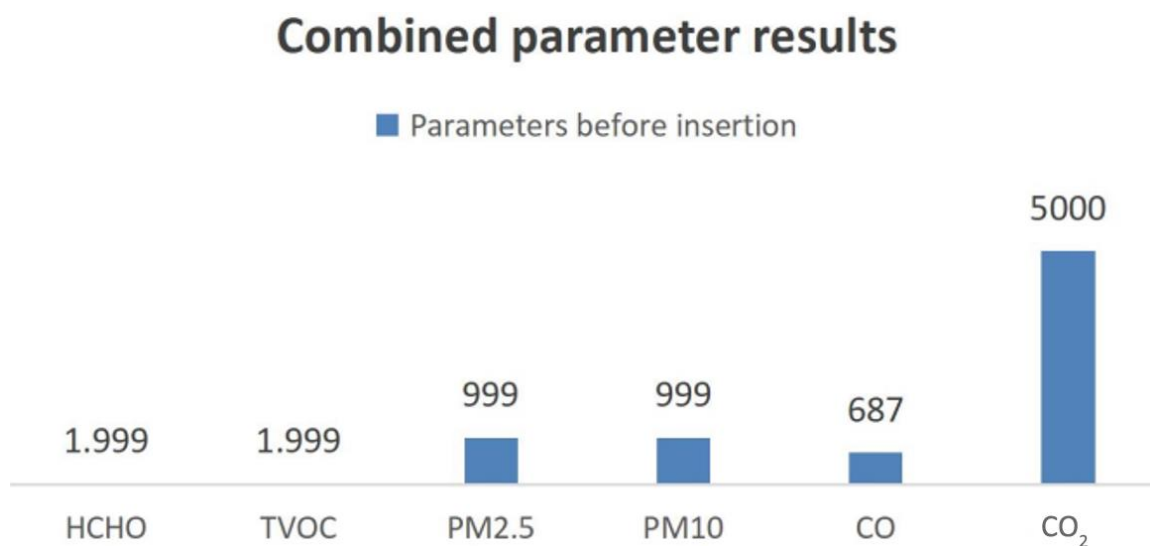

Figure 7. Emission parameter concentrations from generator exhaust after 10 seconds (Before carbon capture insertion).

Figure 7 illustrates the emission parameter concentrations recorded after 10 seconds of generator operation before inserting the carbon capture device.

3.2. Post-Capture Experimental Readings

Before taking new measurements, the air quality detector was reset to ensure that readings returned to normal atmospheric baseline values. The generator was then operated with the carbon capture machine connected to its exhaust outlet, and readings were taken after 10 seconds. From Table 3, we can notice a notable reduction was observed in all measured parameters except TVOC, which remained unchanged. Concentrations of CO and CO_2, the primary focus of this study, decreased significantly, indicating effective adsorption by the biochar-packed chambers within the carbon capture machine.

Table 3. Detector readings after connecting the carbon capture machine to the generator exhaust (t = 10 s).

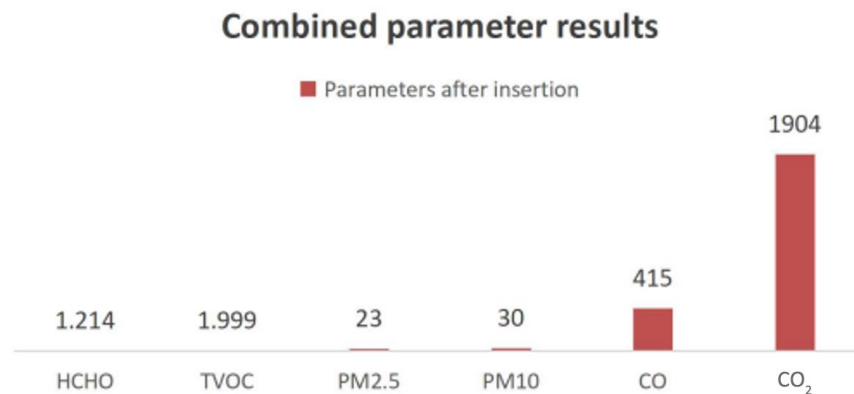| Parameters	Values after t = 10 seconds
HCHO (mg/m³)	1.214
TVOC (mg/m³)	1.999
PM2.5 (μ /m³)	23
PM10 (μ /m³)	30
CO (PPM)	415
CO_2 (PPM)	1904

Figure 8. Column chart of emission concentrations after connecting the carbon capture machine (t = 10 s).

Figure 8 presents the emission concentrations measured after connecting the carbon capture machine, showing reductions across most parameters.
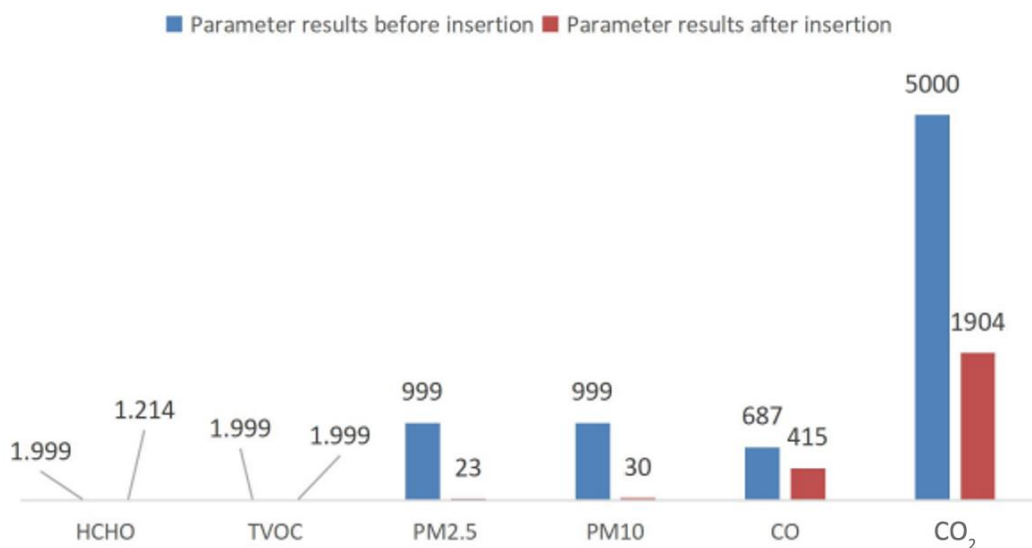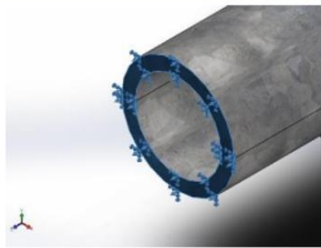

Figure 9. Comparative column chart of emission parameters before and after connecting the carbon capture machine (t = 10 s).

127

Figure 9 compares the emission parameters before and after the carbon capture integration, revealing significant improvements in exhaust quality.

3.3. Emission Test Result Comparison

Figure 9 compares the emission parameter readings obtained before and after connecting the carbon capture machine. The results show a clear reduction in CO, CO_2, $PM_{2.5}$, PM_{10}, and HCHO concentrations following insertion of the device, confirming its functional effectiveness in mitigating gaseous and particulate emissions. Although the detector reached its upper limit during the initial test, the post-insertion readings clearly demonstrate improved exhaust quality.

Fixture name	Fixture Image	Fixture Details		
Fixed-1		**Entities:** 1 face(s) **Type:** Fixed Geometry		
Resultant Forces				
Components	**X**	**Y**	**Z**	**Resultant**
Reaction force(N)	-2.38419e-07	4.32134e-07	-115.765	115.765
Reaction Moment(N.m)	0	0	0	0

Figure 10. Reaction forces at the fixed face.

Figure 10 shows the reaction forces at the fixed face of the inlet port, indicating that the primary resistance occurs in the Z-direction.

3.4. Simulation Results

3.4.1. Resultant Forces and Structural Stability

From Figure 10, the simulation output for the Fixed-1 boundary condition shows that the constrained face primarily resisted load in the Z-direction, with a reaction force of approximately −115.8 N. In contrast, the reaction forces in the X and Y directions were extremely small (on the order of 10^{-7} N), indicating negligible lateral loads.

This distribution suggests that the applied loading and overall structural response are predominantly axial, with minimal transverse or shear components. The fixed face successfully restrained motion in all directions, but only significant resistance was needed along the Z-axis, where the main external load acted.

Furthermore, the reaction moments (0 N·m) about all three axes confirm that the fixed boundary did not experience noticeable rotational effects or twisting moments. This means the applied loading was well-aligned with the model's geometry and load path, producing pure axial deformation without significant bending or torsion.
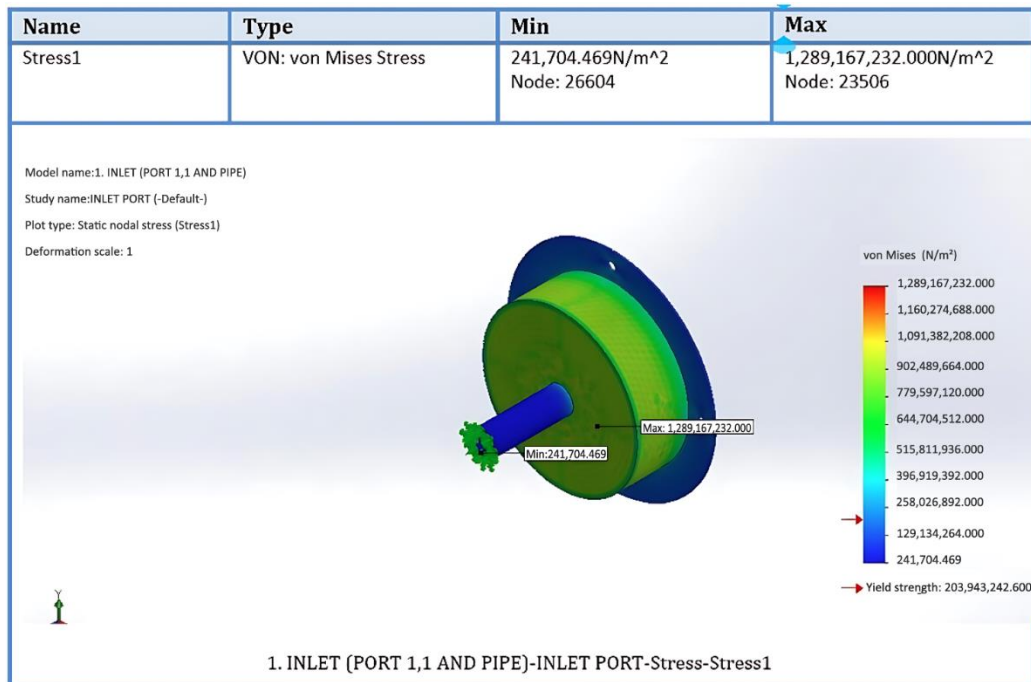
Name	Type	Min	Max
Stress1	VON: von Mises Stress	241,704.469N/m^2 Node: 26604	1,289,167,232.000N/m^2 Node: 23506

Model name:1. INLET (PORT 1,1 AND PIPE)

Study name:INLET PORT (-Default-)

Plot type: Static nodal stress (Stress1)

Deformation scale: 1

von Mises (N/m²)

1,289,167,232.000
1,160,274,688.000
1,091,382,208.000
902,489,664.000
779,597,120.000
644,704,512.000
515,811,936.000
396,919,392.000
258,026,892.000
129,134,264.000
241,704.469

Yield strength: 203,943,242.600

Max: 1,289,167,232.000
Min:241,704.469

1. INLET (PORT 1,1 AND PIPE)-INLET PORT-Stress-Stress1

Figure 11. Von Mises stress distribution for the inlet port assembly.

Figure 11 presents the von Mises stress distribution, highlighting critical regions where stress concentration occurs at the pipe–body junction.

3.4.2. Von Mises Stress

Figure 11 shows that the von Mises stress distribution ranged from 2.42×10^5 N/m² to 1.29×10^9 N/m², with the highest stress observed at the pipe–body junction.

This peak value exceeds the stainless-steel yield strength ($\approx 2.04 \times 10^8$ N/m²), indicating that localized stress concentration could lead to structural failure under the current loading.

Therefore, design modifications such as increasing wall thickness or improving joint curvature are necessary to enhance safety and reliability.
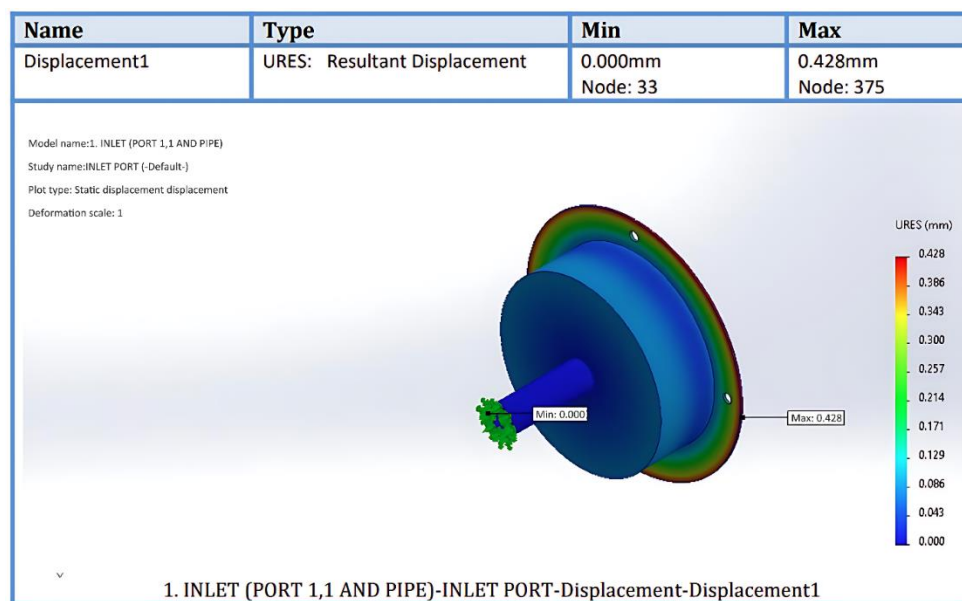
Name	Type	Min	Max
Displacement1	URES: Resultant Displacement	0.000mm Node: 33	0.428mm Node: 375

Model name:1. INLET (PORT 1,1 AND PIPE)

Study name:INLET PORT (-Default-)

Plot type: Static displacement displacement

Deformation scale: 1

URES (mm)

0.428
0.386
0.343
0.300
0.257
0.214
0.171
0.129
0.086
0.043
0.000

Min: 0.000
Max: 0.428

1. INLET (PORT 1,1 AND PIPE)-INLET PORT-Displacement-Displacement1

Figure 12. Resultant displacement distribution for the inlet port assembly.

Figure 12 illustrates the resultant displacement distribution under combined thermal and pressure loading, showing minimal deformation.

3.4.3. Resultant Displacement

The displacement contour in Figure 12 showed minimal overall deformation under combined thermal and pressure loads. The maximum displacement was approximately 0.43 mm, occurring near the inlet rim, while the fixed boundary remained stable.

This small displacement relative to component dimensions indicates mechanical stability, suggesting that the inlet structure can maintain its shape and sealing performance during operation.
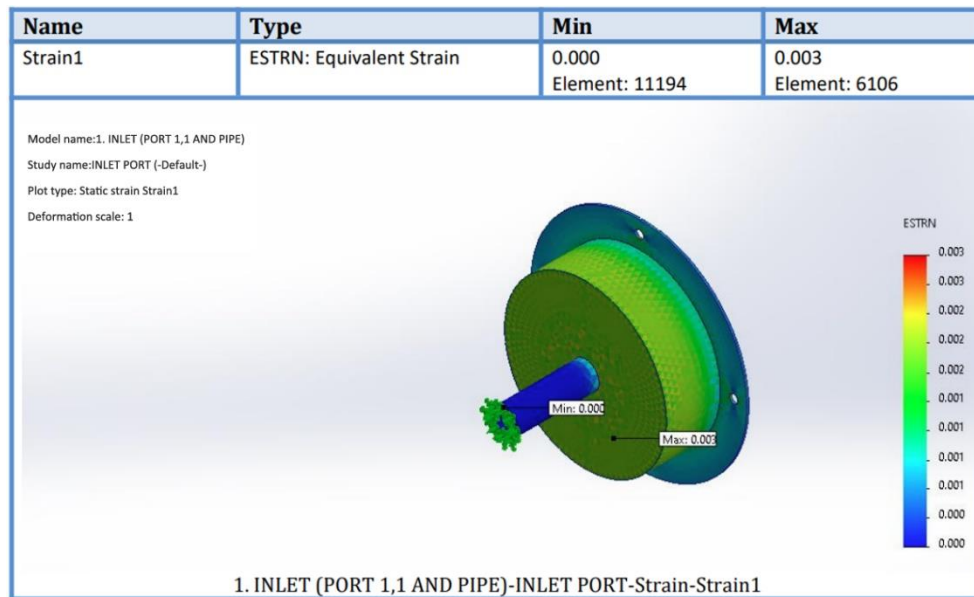
Name	Type	Min	Max
Strain1	ESTRN: Equivalent Strain	0.000 Element: 11194	0.003 Element: 6106

Figure 13. Strain distribution for the inlet port assembly.

Figure 13 displays the equivalent strain distribution for the inlet port assembly, indicating that the strains remain within the elastic limit.

3.4.4. Equivalent Strain

The equivalent strain ranged from 0.000 to 0.003, with higher values concentrated in regions exposed to direct loading. Since these strain values remain within the elastic range, the structure is not expected to undergo permanent deformation. This confirms that, apart from localized stress concentration, the overall inlet port design is structurally sound for the applied thermal and pressure conditions.

3.5. Comparison of Theoretical and Simulation Results

Substituting the design parameters into the analytical equation yields a hoop stress of -4.79×10^6 N/m². The negative value indicates compressive stress, confirming that the external atmospheric pressure exceeds the internal back pressure from the exhaust gas.

This means that the chamber walls are subjected to inward compression rather than outward expansion, validating that the selected wall thickness of 0.3 cm provides sufficient strength under the given loading conditions.

3.6. Interpretation and Implications

- The simulation findings aligned with the theoretical analysis, confirming the structural adequacy of the inlet port design.

- The compressive stress state ensures that the chamber is not at risk of bursting or deformation under exhaust pressure.
- Operational safety is primarily governed by thermal stress effects rather than internal pressure.

4. CONCLUSION

This study successfully designed, fabricated, and tested a small-scale carbon capture device for generator exhaust applications. The system was developed using stainless-steel chambers packed with biochar as the adsorbent medium. Experimental validation demonstrated a significant reduction in carbon monoxide (CO) and carbon dioxide (CO_2) concentrations after the exhaust gases passed through the capture chambers, confirming the adsorption effectiveness of biochar in mitigating harmful emissions.

Static simulation analysis using SolidWorks further verified the mechanical integrity of the inlet port under combined thermal and pressure loading. Although localized stress concentrations exceeded the material's yield strength, the overall deformation and strain values remained within the elastic limit, indicating satisfactory operational stability under moderate conditions.

Theoretical and numerical analyses agreed that the selected wall thickness of 0.3 cm was structurally adequate to withstand compressive loading resulting from the external atmospheric pressure dominance. Collectively, these results establish the prototype's functional feasibility and mechanical soundness for small-scale emission reduction applications.

5. RECOMMENDATION

Based on the results of this study, it is recommended that future designs incorporate a slightly increased wall thickness or the use of reinforced stainless-steel materials at critical junctions to mitigate stress concentration and enhance structural durability. The use of activated or chemically modified biochar is also advised to increase surface area and improve adsorption efficiency. For improved accuracy and operational insight, the inclusion of digital gas sensors with data-logging capabilities is recommended to enable continuous monitoring of emission levels during operation. Further testing should be conducted under extended generator operation and varying load conditions to evaluate the long-term performance and regeneration potential of the biochar adsorbent. Finally, the developed carbon capture system could be integrated with renewable energy technologies such as biomass or biogas generators to support sustainable, low-carbon energy production and contribute to localized environmental management efforts.

REFERENCES

Adenikinju, A. F. (2003). Electric infrastructure failures in Nigeria: A survey-based analysis of the costs and adjustment responses. *Energy Policy, 31*(14), 1519-1530. https://doi.org/10.1016/S0301-4215(02)00208-2

Ahmed, I., Rehan, M., Basit, A., & Hong, K.-S. (2022). Greenhouse gases emission reduction for electric power generation sector by efficient dispatching of thermal plants integrated with renewable systems. *Scientific Reports, 12*(1), 12380. https://doi.org/10.1038/s41598-022-15983-0

Allangawi, A., Alzaimoor, E. F., Shanaah, H. H., Mohammed, H. A., Saqer, H., El-Fattah, A. A., & Kamel, A. H. (2023). Carbon capture materials in post-combustion: Adsorption and absorption-based processes. *Journal of Carbon Research*, *9*(1), 17. https://doi.org/10.3390/c9010017

Bai, Q., & Bai, Y. (2014). Introduction. In Subsea pipeline design, analysis, and installation. In (pp. 3–21). Netherlands: Elsevier. https://doi.org/10.1016/B978-0-12-386888-6.00001-8

Chao, C., Deng, Y., Dewil, R., Baeyens, J., & Fan, X. (2021). Post-combustion carbon capture. *Renewable and Sustainable Energy Reviews*, *138*, 110490. https://doi.org/10.1016/j.rser.2020.110490

El Zein, A. L., & Chehayeb, N. A. (2015). The effect of greenhouse gases on earth's temperature. *International Journal of Environmental Monitoring and Analysis*, *3*(2), 74-79. https://doi.org/10.11648/j.ijema.20150302.16

Gkotsis, P., Peleka, E., & Zouboulis, A. (2023). Membrane-based technologies for post-combustion CO_2 capture from flue gases: Recent progress in commonly employed membrane materials. *Membranes*, *13*(12), 898. https://doi.org/10.3390/membranes13120898

González, A., Plaza, M. G., Rubiera, F., & Pevida, C. (2013). Sustainable biomass-based carbon adsorbents for post-combustion CO_2 capture. *Chemical Engineering Journal*, *230*, 456-465. https://doi.org/10.1016/j.cej.2013.06.118

Herzog, H. J. (2018). *Carbon capture*. United States: MIT Press. https://doi.org/10.7551/mitpress/11423.001.0001

Hua, W., Sha, Y., Zhang, X., & Cao, H. (2023). Research progress of carbon capture and storage (CCS) technology based on the shipping industry. *Ocean Engineering*, *281*, 114929. https://doi.org/10.1016/j.oceaneng.2023.114929

McKendry, P. (2002). Energy production from biomass (part 1): Overview of biomass. *Bioresource Technology*, *83*(1), 37-46. https://doi.org/10.1016/S0960-8524(01)00118-3

Peu, S. D., Das, A., Hossain, M. S., Akanda, M. A. M., Akanda, M. M. H., Rahman, M., . . . Salah, M. M. (2023). A comprehensive review on recent advancements in absorption-based post combustion carbon capture technologies to obtain a sustainable energy sector with clean environment. *Sustainability*, *15*(7), 5827. https://doi.org/10.3390/su15075827

Raganati, F., Miccio, F., & Ammendola, P. (2021). Adsorption of carbon dioxide for post-combustion capture: A review. *Energy & Fuels*, *35*(16), 12845-12868. https://doi.org/10.1021/acs.energyfuels.1c01618

Reddy, A. C. (2005). *Prediction of bursting pressure of thin walled 316 stainless steel tubes based on ASME B31G criterion*. Paper presented at the National Conference on Advances in Design Approaches and Production Technologies (ADAPT-2005).

Sharma, R., & Tyagi, S.K. (2024). Post combustion carbon capture using chemical absorption: A short review. *International Journal of Ambient Energy*, *45*(1), 2360999. https://doi.org/10.1080/01430750.2024.2360999

Tian, Z., Wang, Y., Zhen, X., & Liu, Z. (2022). The effect of methanol production and application in internal combustion engines on emissions in the context of carbon neutrality: A review. *Fuel*, *320*, 123902. https://doi.org/10.1016/j.fuel.2022.123902

Wang, J., & Azam, W. (2024). Natural resource scarcity, fossil fuel energy consumption, and total greenhouse gas emissions in top emitting countries. *Geoscience Frontiers*, *15*(2), 101757. https://doi.org/10.1016/j.gsf.2023.101757

Wilcox, J. (2012). *Carbon capture*. Germany: Springer. https://doi.org/10.1007/978-1-4614-2215-0